

## Research Paper

# Synthesis of enantiopure $^{18}\text{F}$ -trifluoromethyl cysteine as a structure-mimetic amino acid tracer for glioma imaging

Shaoyu Liu<sup>1\*</sup>, Hui Ma<sup>1\*</sup>, Zhanwen Zhang<sup>1,3</sup>, Liping Lin<sup>1</sup>, Gongjun Yuan<sup>1</sup>, Xiaolan Tang<sup>4</sup>, Dahong Nie<sup>5</sup>, Shende Jiang<sup>6</sup>, Guang Yang<sup>2</sup>✉, Ganghua Tang<sup>1</sup>✉

1. Department of Nuclear Medicine, Guangdong Engineering Research Center for Translational Application of Medical Radiopharmaceuticals, The First Affiliated Hospital, Sun Yat-sen University, Guangzhou 510080, People's Republic of China.
2. The State Key Laboratory of Medicinal Chemical Biology, College of Pharmacy, Nankai University, Tianjin 300350, People's Republic of China.
3. Department of Nuclear Medicine, The Sixth Affiliated Hospital, Sun Yat-sen University, Guangzhou 510655, People's Republic of China.
4. College of Materials and Energy, South China Agricultural University, Guangzhou 510642, People's Republic of China.
5. Department of Radiation Oncology, The First Affiliated Hospital, Sun Yat-sen University, Guangzhou 510080, People's Republic of China.
6. School of Pharmaceutical Science and Technology, Tianjin University, Tianjin 300072, People's Republic of China.

\*These authors contributed equally.

✉ Corresponding author: Guang.Yang@nankai.edu.cn; tangghua@mail.sysu.edu.cn.

© Ivyspring International Publisher. This is an open access article distributed under the terms of the Creative Commons Attribution (CC BY-NC) license (<https://creativecommons.org/licenses/by-nc/4.0/>). See <http://ivyspring.com/terms> for full terms and conditions.

Received: 2018.08.22; Accepted: 2019.01.05; Published: 2019.01.30

## Abstract

Although  $^{11}\text{C}$ -labelled sulfur-containing amino acids (SAAs) including L-methyl- $^{11}\text{C}$ methionine and S- $^{11}\text{C}$ -methyl-L-cysteine, are attractive tracers for glioma positron emission tomography (PET) imaging, their applications are limited by the short half-life of the radionuclide  $^{11}\text{C}$  ( $t_{1/2} = 20.4$  min). However, development of  $^{18}\text{F}$ -labelled SAAs ( $^{18}\text{F}$ ,  $t_{1/2} = 109.8$  min) without significant structural changes or relying on prosthetic groups remains to be a great challenge due to the absence of adequate space for chemical modification.

**Methods:** We herein present  $^{18}\text{F}$ -trifluoromethylated D- and L-cysteines which were designed by replacing the methyl group with  $^{18}\text{F}$ -trifluoromethyl group using a structure-based bioisosterism strategy. These two enantiomers were synthesized stereoselectively from serine-derived cyclic sulfamidates *via* a nucleophilic  $^{18}\text{F}$ -trifluoromethylthiolation reaction followed by a deprotection reaction. Furthermore, we conducted preliminary *in vitro* and *in vivo* studies to investigate the feasibility of using  $^{18}\text{F}$ -trifluoromethylated cysteines as PET tracers for glioma imaging.

**Results:** The two-step radiosynthesis provided the desired products in excellent enantiopurity (ee > 99%) with  $14\% \pm 3\%$  of radiochemical yield. *In vitro* cell study demonstrated that both enantiomers were taken up efficiently by C6 tumor cells and were mainly transported by systems L and ASC. Among them, the D-enantiomer exhibited relatively good stability and high tumor-specific accumulation in the animal studies.

**Conclusion:** Our findings indicate that  $^{18}\text{F}$ -trifluoromethylated D-cysteine, a new SAA tracer, may be a potential candidate for glioma imaging. Taken together, our study represents a first step toward developing  $^{18}\text{F}$ -trifluoromethylated cysteines as structure-mimetic tracers for PET tumor imaging.

Key words: Positron emission tomography,  $^{18}\text{F}$ -trifluoromethylthiolation,  $^{18}\text{F}$ -trifluoromethylated cysteine,  $^{18}\text{F}$ -labelled sulfur-containing amino acid, glioma imaging

## Introduction

Amino acids (AAs) enter cells *via* transport mediated by specific plasmatic membrane proteins [1, 2], also known as AA transporters that are highly up-regulated in various malignant tumors in comparison to normal tissues (*e.g.*, systems L, ASC, and A) [3-9]. Targeting the elevated expression of AA

transporters is an effective way to design the radiolabelled AAs as tumor-specific imaging tracers. No surprise, positron-labelled AAs have been an important class of radiopharmaceuticals for positron emission tomography (PET) imaging of cancer (*e.g.*, prostate, breast, and brain cancer) [10-17].

Initial applications and studies mainly focused on the naturally occurring AAs, because carbon-11 ( $^{11}\text{C}$ ) can be easily incorporated into AAs without any effects on biological properties [18-21]. Sulfur-containing AAs (SAAs) play many physiological and metabolic roles in living systems, such as protein synthesis, methylation of DNA, and biosynthesis of glutathione [22]. L-methyl- $^{11}\text{C}$ methionine ( $^{11}\text{C}$ MET, **Figure S1A**), an essential SAA labelled with  $^{11}\text{C}$ , has been extensively used for brain tumor imaging [23-27]. Compared with clinically used 2- $^{18}\text{F}$ fluoro-2-deoxy-D-glucose ( $^{18}\text{F}$ FDG),  $^{11}\text{C}$ MET accumulates preferentially in tumor cells but poorly in normal brain cells, thus providing a higher sensitivity to detect brain tumors [26, 28, 29]. However,  $^{11}\text{C}$ MET is taken up not only by tumors but also by other inflammatory lesions, leading to low tumor specificity [30-33]; additionally, it is susceptible to *in vivo* metabolism [34], complicating kinetic analysis. To address these deficiencies, S- $^{11}\text{C}$ -methyl-L-cysteine **1L** (S- $^{11}\text{C}$ CH<sub>3</sub>-L-CYS) and S- $^{11}\text{C}$ -methyl-D-cysteine **1D** (S- $^{11}\text{C}$ CH<sub>3</sub>-D-CYS), a pair of  $^{11}\text{C}$ -labelled S-methylcysteine enantiomers (**Figure 1A** and **Figure S1B**), were successively developed *via*  $^{11}\text{C}$ -isotopic substitution in our previous studies [35-38]. Preliminary studies indicated that the tracers were superior to  $^{18}\text{F}$ FDG and  $^{11}\text{C}$ MET in the differentiation of tumor from inflammation [35, 36, 38-40]. Nevertheless, the short half-life of  $^{11}\text{C}$  ( $t_{1/2} = 20.4$  min) restricts the widespread application of these tracers, resulting in an urgent demand for  $^{18}\text{F}$ -labelled SAA tracers ( $^{18}\text{F}$ ,  $t_{1/2} = 109.8$  min).

To date, most previous studies on the  $^{18}\text{F}$ -labelled SAA tracers (**Figure S1B**) have

concentrated on molecular scaffolds which can be readily radiolabelled by linking with a prosthetic group, such as S-(2- $^{18}\text{F}$ fluoroethyl)-L-homocysteine [41, 42], S-(3- $^{18}\text{F}$ fluoropropyl)-L-homocysteine [43], S-(3- $^{18}\text{F}$ fluoropropyl)-D-homocysteine [43, 44]. For the structure-sensitive SAA molecules, however, even minor side-chain alterations caused by the prosthetic groups (S-ethyl and S-propyl) may lead to significant changes in biological properties. More recently, to avoid affecting the biological activity,  $^{18}\text{F}$ -B-MET (a methionine boramino acid derivative; **Figure S1B**) was developed as a potential substitute of  $^{11}\text{C}$ MET by isosteric substitution of carboxylate ( $-\text{CO}_2^-$ ) group with trifluoroborate ( $-\text{BF}_3^-$ ) group [45].  $^{18}\text{F}$ -B-MET shared the same AA transport systems with  $^{11}\text{C}$ MET owing to the nearly identical charge distribution patterns. But these groups ( $-\text{BF}_3^-$  and  $-\text{CO}_2^-$ ) differ considerably in chemical structure and properties, which may cause potential differences in metabolism of the tracers *in vivo*. Therefore, despite these undeniable successes, the development of  $^{18}\text{F}$ -labelled SAA tracers without significant structural changes or relying on prosthetic groups remains to be a great challenge, highlighting the importance of research on a structure-mimetic tracer.

Trifluoromethyl ( $-\text{CF}_3$ ), the smallest symmetrical multi-fluorine group, has captured intense attention in the fields of chemistry and pharmacy, because of its ability to increase chemical and metabolic stability, to improve bioavailability and lipophilicity, and to enhance binding selectivity [46-50]. Given these advantages of  $-\text{CF}_3$  and our interest in  $^{18}\text{F}$ -labelled SAA tracers, in this work, we aimed to develop a couple of  $^{18}\text{F}$ -trifluoromethylated cysteine enantiomers for PET imaging of glioma. As shown in

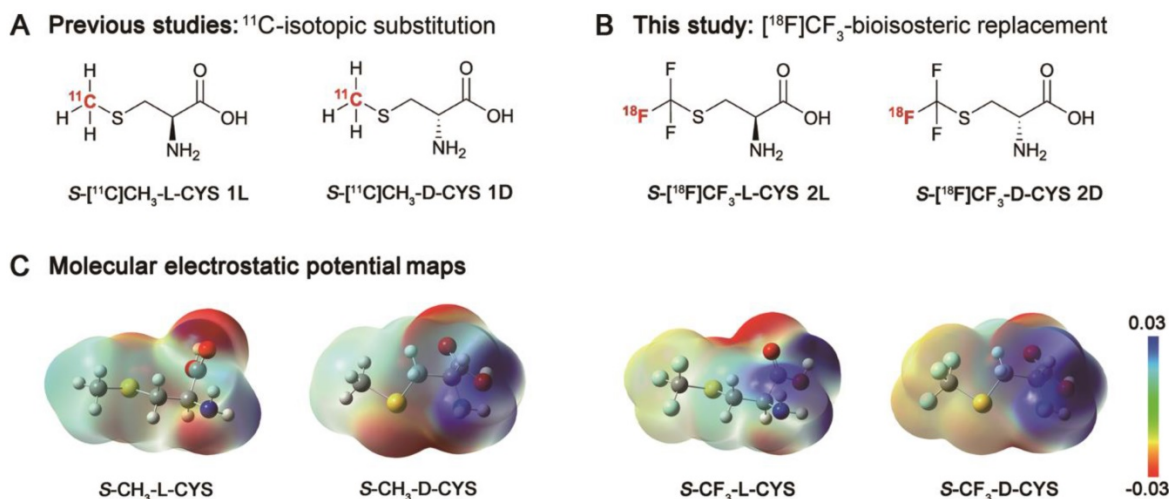


**Figure 1.** (A) Chemical structures of S- $^{11}\text{C}$ CH<sub>3</sub>-L-CYS **1L** and S- $^{11}\text{C}$ CH<sub>3</sub>-D-CYS **1D** using isotopic substitution of  $-\text{CH}_3$  with  $-\text{[}^{11}\text{C]CH}_3$  in our previous studies; (B) Chemical structures of S- $^{18}\text{F}$ CF<sub>3</sub>-L-CYS **2L** and S- $^{18}\text{F}$ CF<sub>3</sub>-D-CYS **2D** using bioisosteric replacement of  $-\text{CH}_3$  with  $-\text{[}^{18}\text{F]CF}_3$  in this study; (C) Molecular electrostatic potential (MEP) maps of S-CH<sub>3</sub>-L-CYS, S-CH<sub>3</sub>-D-CYS and their mimics were carried out at the B3LYP/6-31 G (d, p) level using the Gaussian<sup>®</sup> 09W computational package in the water phase (the blue indicates the distribution of positive charge, and the red indicates the distribution of negative charge). As shown, S-CF<sub>3</sub>-L-CYS and S-CF<sub>3</sub>-D-CYS are nearly identical in structural arrangement and charge distribution pattern to S-CH<sub>3</sub>-L-CYS and S-CH<sub>3</sub>-D-CYS, respectively.

**Figure 1B**,  $S$ - $^{18}\text{F}$  $\text{CF}_3$ -L-CYS **2L** and  $S$ - $^{18}\text{F}$  $\text{CF}_3$ -D-CYS **2D** were designed by replacement of methyl ( $-\text{CH}_3$ ) group with  $-\text{CF}_3$  group according to a structure-based bioisosterism strategy. Encouragingly, this proposal received great support from the calculated molecular electrostatic potential (MEP) maps of the  $S$ -methylcysteines and their mimics (**Figure 1C**). Herein, we report the synthesis of enantiopure **2L** and **2D** starting from serine-derived cyclic-sulfamidates *via* a nucleophilic  $^{18}\text{F}$ -trifluoromethylthiolation reaction, and also describe preliminary *in vitro* and *in vivo* biological evaluation.

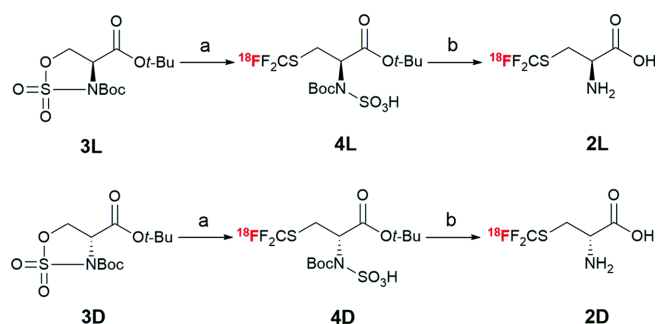
## Results and Discussion

### Radiochemistry

Although the development of the  $^{18}\text{F}$ -trifluoromethylated SAA tracers is conceptually straightforward, it is actually quite challenging due to the difficulty of introducing fluorine-18 into the radiolabelled  $-\text{SCF}_3$  group. The most efficient synthetic routes toward non-labelled trifluoromethylated SAAs involve direct trifluoromethylation of thiols using electrophilic trifluoromethylating reagents, such as the Togni's [51, 52] and Umemoto's [53] reagents. However, until recently, only one such radiolabelled reagent ( $^{18}\text{F}$ -Umemoto's reagent) was successfully developed for electrophilic  $^{18}\text{F}$ -trifluoromethylation [54]. In addition, Liang and Xiao reported a nucleophilic  $^{18}\text{F}$ -trifluoromethylthiolation of  $\alpha$ -bromo carbonyl compounds and aliphatic halides with difluorocarbene (generated from  $\text{Ph}_3\text{P}^+\text{CF}_2\text{CO}_2^-$ ; PDFFA) in the presence of  $^{18}\text{F}$ -fluoride and elemental sulfur ( $\text{S}_8$ ) [55, 56]. Cahard and Ma recently developed a straightforward method for the synthesis of  $\beta$ - and  $\gamma$ - $\text{SCF}_3$   $\alpha$ -AA derivatives through nucleophilic trifluoromethylthiolation of cyclic sulfamidates [57]. Moreover, serine-derived cyclic sulfamidates have been widely used as configurationally stable chiral building blocks for the synthesis of enantiopure  $\beta$ -substituted  $\alpha$ -AAs [57-59]. Inspired by these studies, we envisioned that the  $^{18}\text{F}$ -trifluoromethylated SAAs **2L** and **2D** could be synthesized stereoselectively from serine-derived cyclic sulfamidates *via* a nucleophilic  $^{18}\text{F}$ -trifluoromethylthiolation reaction followed by a deprotection reaction.

The initial step in our work was to synthesize the cyclic sulfamidates **3L** and **3D** *via* a four-step reaction (**Scheme S1**), according to the reported methods [12, 58, 60-62]. With the desired cyclic-sulfamidates in hand, we set out to optimize the reaction conditions (**Table S1**) and to explore the synthesis of **2L** and **2D**. As shown in **Scheme 1**, the  $^{18}\text{F}$ -trifluoromethyl-

thiolation of cyclic-sulfamidates **3L** and **3D** (2 mg, 6  $\mu\text{mol}$ ) with PDFFA (1.5 mg, 6  $\mu\text{mol}$ ) and  $\text{S}_8$  (3.0 mg, 12  $\mu\text{mol}$ ) in the presence of heating-block-dried  $\text{K}_{2.2.2}/\text{K}^{18}\text{F}$  was carried out at 70  $^\circ\text{C}$  for 5 min to give the radiolabelled intermediates **4L** and **4D** which were subsequently purified by the C18 cartridge and eluted with ethanol. Then, the solution was evaporated and hydrolyzed in 4N HCl aq. at 90  $^\circ\text{C}$  for 10 min [61, 62]. Finally, the desired products **2L** and **2D** were neutralized ( $\text{pH} \approx 6$ ) and isolated using solid phase extraction to obtain  $14\% \pm 3\%$  RCY ( $n = 6$ ) in 35 min. The radiochemical purity was higher than 98%, as determined by radio-TLC (**Figure S2-3**) [63]. Similar to a previous report about the synthesis of non-radiolabelled L-trifluoromethylcysteine [64], the harsh hydrolysis conditions failed to lead to a  $\beta$ -elimination side reaction, suggesting a good stability of **2L** and **2D** in acidic conditions. **2L** and **2D** had  $\log P$  values of -2.75 and -2.22, respectively, and were  $> 95\%$  stable in PBS at 37  $^\circ\text{C}$  for up to 2 hours (**Figure S5**). According to the chiral radio-HPLC analysis, almost no racemization was detected during the synthesis of **2L** and **2D** (optical purity:  $ee > 99\%$ ; **Figure 2** and **Figure S4**), which forcefully confirmed the feasibility of this nucleophilic  $^{18}\text{F}$ -trifluoromethylthiolation protocol (**Scheme S2**) for synthesizing enantiopure  $^{18}\text{F}$ -trifluoromethylated cysteines.



**Scheme 1.** Synthesis of  $^{18}\text{F}$ -trifluoromethyl cysteine enantiomers **2L** and **2D** *via* nucleophilic  $^{18}\text{F}$ -trifluoromethylthiolation. Reagents and conditions: a. PDFFA,  $\text{S}_8$ ,  $\text{K}_{2.2.2}/\text{K}^{18}\text{F}$ ,  $\text{CH}_3\text{CN}$ , 70  $^\circ\text{C}$ , 5 min; b. 4N HCl aq., 90  $^\circ\text{C}$ , 10 min.

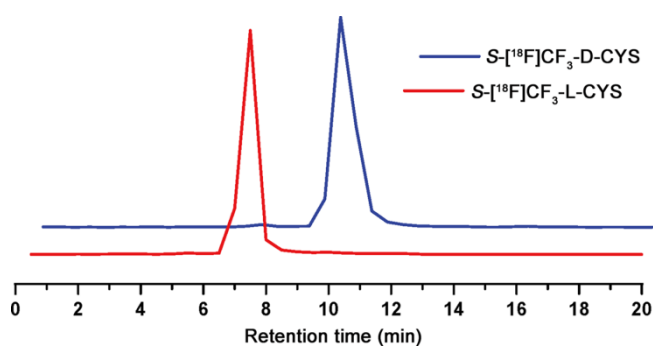


**Figure 2.** Chiral radio-HPLC analysis of **2L** and **2D** (test tube method<sup>#</sup>).

### In vitro cell research

Encouraged by the successful synthesis of **2L** and **2D**, we conducted *in vitro* cell uptake study to explore the specificity of each enantiomer. As shown in **Figure 3A**, the uptake of **2L** in C6 cells increased steadily in a time-dependent manner, and the maximal value (4.33% uptake/100  $\mu\text{g}$  protein) appeared at the 120 min. **2D** rapidly accumulated in the cells within a short time and reached a maximum of about 6.34% uptake/100  $\mu\text{g}$  protein after incubation for 20 min, but then declined slowly afterward. One possible reason for the above situation was that **2D** was being transported into/out of the C6 cells at a higher rate compared with **2L**. Thus, the uptake of **2L** was higher than that of **2D** in C6 cells after approximately 60 min, and the uptake difference was gradually enlarged with the prolonged incubation time. *In vitro* cell uptake studies indicated that cysteines functionalized with an [ $^{18}\text{F}$ ]CF<sub>3</sub> moiety could be taken up efficiently by C6 cells, but there was an obvious distinction between different chiral isomers on the cellular uptake efficiency.

Although mammalian cells generally tend to employ L-enantiomer for the biological basic needs, both the enantiomers of AAs can be transported [44]. In order to investigate the uptake mechanism of each enantiomer, a competitive inhibition study was performed using C6 glioma cells in the presence of AA transporter inhibitors (**Figure 3B-C**). After 15 min of incubation in choline chloride solution (-Na<sup>+</sup>), the cellular uptake of **2L** and **2D** was obviously decreased by BCH (2-amino-2-norbornanecarboxylic acid), a classical inhibitor for system L transporters. Additionally, the transportation of **2L** and **2D** in saline solution (+Na<sup>+</sup>) was effectively blocked by L-serine (Ser), a non-specific inhibitor for system ASC transporters [36, 65]. By contrast, MeAIB (2-aminoisobutyric acid), a system A inhibitor, exerted almost no significant effect on the transportation of **2L** and **2D** into the cells in either choline chloride or saline solution. Similar to <sup>11</sup>C-methyl-cysteines **1L** and **1D** [35, 36], we found that the cellular uptake of both enantiomers of <sup>18</sup>F-trifluoromethylated cysteine in C6 cells mainly relied on the systems L and ASC, however, the system A did not contribute to the radioactive accumulation. Remarkably, the cellular uptake of **2L** was significantly suppressed by L-MCYS (S-methyl-L-cysteine) in both choline chloride and saline solution (**Figure 3B**), strongly suggesting that L-MCYS and its mimic **2L** shared the same AA transport systems.

Next, we examined the extent of protein incorporation of each enantiomer in C6 tumor cells, according to the similar reported method [66]. After precipitation with trichloroacetic acid (TCA), the

protein incorporation of **2L** in C6 cells was 0.6% and 4.5% at 30 and 120 min incubation times (**Figure 3D**), respectively. Thus, there was almost no incorporation of **2L** into protein. In comparison, a markedly higher percentage of **2D** incorporated into protein, with about 5% and 13% at 30 and 120 min, respectively, implying that there were some interactions between **2D** and intracellular macromolecules (perhaps enzymes). Overall, the *in vitro* cell studies fully demonstrated that cellular uptake of <sup>18</sup>F-trifluoromethylated cysteines was mainly associated with their AA transport systems across the cell membrane rather than with the protein incorporation.

### In vivo biodistribution studies

To explore the *in vivo* biodistribution of each enantiomer, we subsequently performed the studies by dissection on normal Kunming mice ( $n = 4$  per group). Surprisingly, a rapid and progressive accumulation of radioactivity was observed in the bone from 5 to 90 min after injection of **2L** (**Figure 4A**). But for **2D**, the bone uptake only slightly increased over time (**Figure 4B**), suggesting a slow defluorination or a bone marrow uptake. Even though both **2L** and **2D** were stable *in vitro*, there was a marked difference in stability between the two enantiomers *in vivo*. One reasonable explanation is that **2L** might serve as a preferential substrate for cysteine S-conjugate  $\beta$ -lyases and underwent an enzyme-catalyzed  $\beta$ -elimination reaction [67, 68]. Structurally, **2D** is also a cysteine S-conjugate but showed relatively good *in vivo* stability, presumably because the  $\beta$ -elimination reaction proceeded with high L-stereoselectivity. On the basis of these analyses, a possible mechanism was proposed to explain the surprising *in vivo* instability of **2L**. As illustrated in **Scheme 2**, the deprotonated base (B) abstracts a proton from **2L** and initiates transaldimination of pyridoxal 5'-phosphate (PLP)-imine with the deprotonated  $\alpha$ -amino group to form the **2L**-PLP Schiff base [69, 70]. The Schiff base is then  $\alpha$ -deprotonated by the  $\epsilon$ -amino group of the lysine residue to give a quinoid intermediate [71, 72]. Subsequent elimination of [ $^{18}\text{F}$ ]trifluoromethanethiol ([ $^{18}\text{F}$ ]CF<sub>3</sub>SH) further decomposes to release <sup>18</sup>F-fluoride; please see the green box in **Scheme 2**) from the  $\beta$ -carbon position produces a ketimine intermediate which is finally hydrolyzed to afford PLP-imine, pyruvate and ammonium [69, 73].

In addition, biodistribution studies by dissection indicated that **2D** was primarily excreted *via* the kidneys (urinary system) and to a minor extent *via* the hepatic route. Fast washout of radioactivity from the main tissues and organs (*e.g.*, blood, heart, lung,

pancreas, and stomach) was observed during the entire experimental process (Figure 4B), revealing that 2D has advantages of rapid *in vivo* clearance. Similar to 1L and 1D [35, 36, 39], low accumulation of 2D in the brain was found in the biodistribution data, which could be considered as an advantage or a disadvantage. It was an advantage because the tracer with low brain uptake would contribute to providing a low background activity for PET imaging of brain tumors. On the other hand, it could also be a disadvantage for the tracer, as the uptake in any

cranial tumor would be low due to a low availability of the tracer after transport through the blood-brain barrier. Moreover, we also performed a comparison between [<sup>18</sup>F]FDG and 2D in Kunming mice (*n* = 4 per group) with turpentine-induced acute inflammation. The preliminary results (data obtained by dissection) showed that 2D had significantly lower inflammation/muscle and inflammation/blood ratios than [<sup>18</sup>F]FDG at 60 min post-injection (Table S2), which was similar to our previous report on 1D [40].

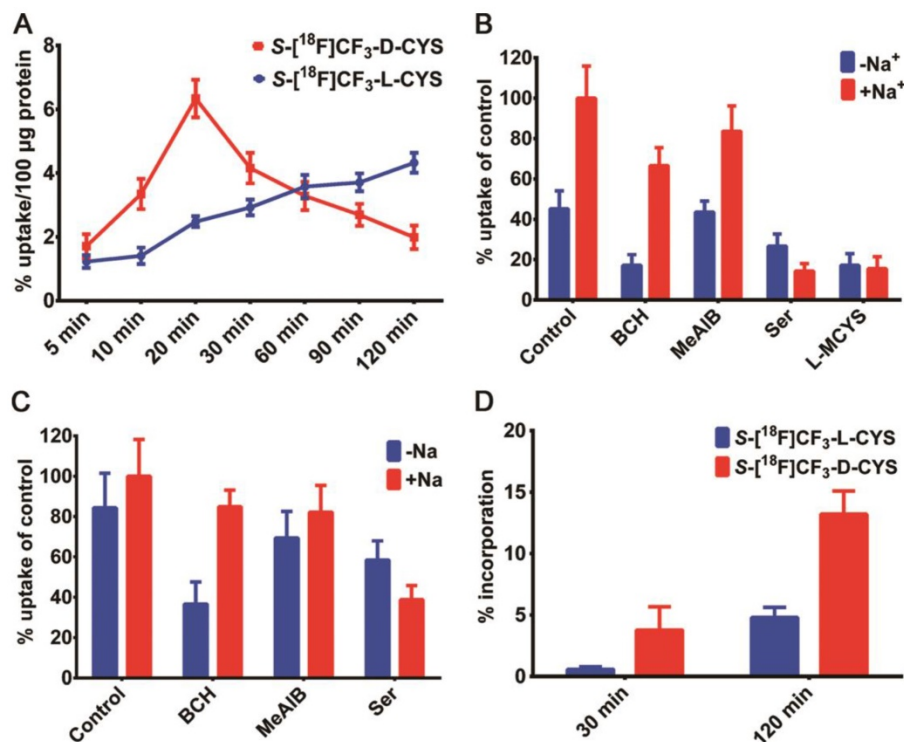


**Figure 3.** (A) Time-dependent cell uptake assays with 2L and 2D in C6 cells; (B) Competitive inhibition of C6 cell uptake of S-[<sup>18</sup>F]CF<sub>3</sub>-L-CYS 2L after co-incubation with each inhibitor or L-MCYS for 15 min; (C) Competitive inhibition of C6 cell uptake of S-[<sup>18</sup>F]CF<sub>3</sub>-D-CYS 2D after co-incubation with each inhibitor for 15 min; (D) The comparison of protein incorporation of 2L and 2D in C6 tumor cell line after incubation for 30 min and 120 min.

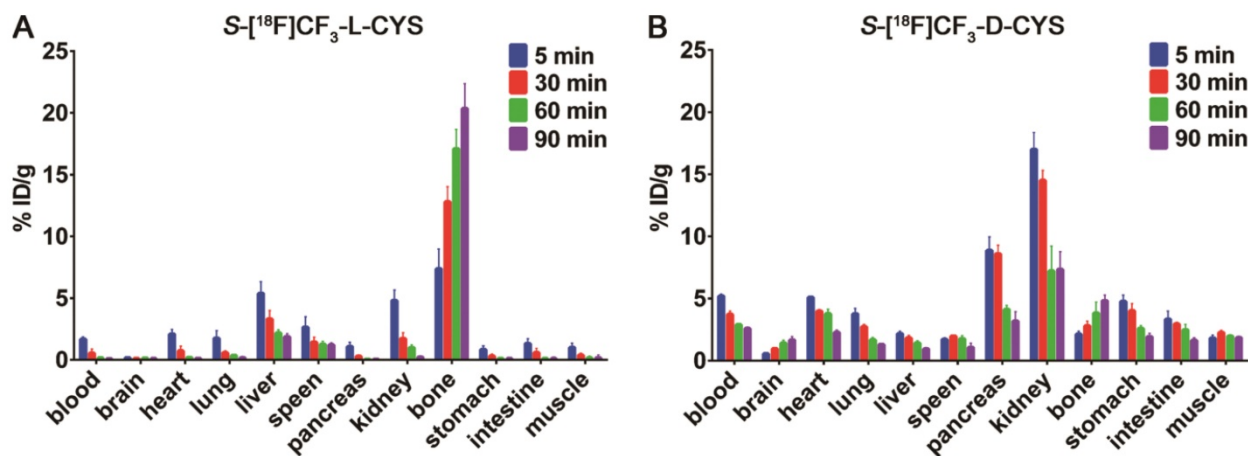
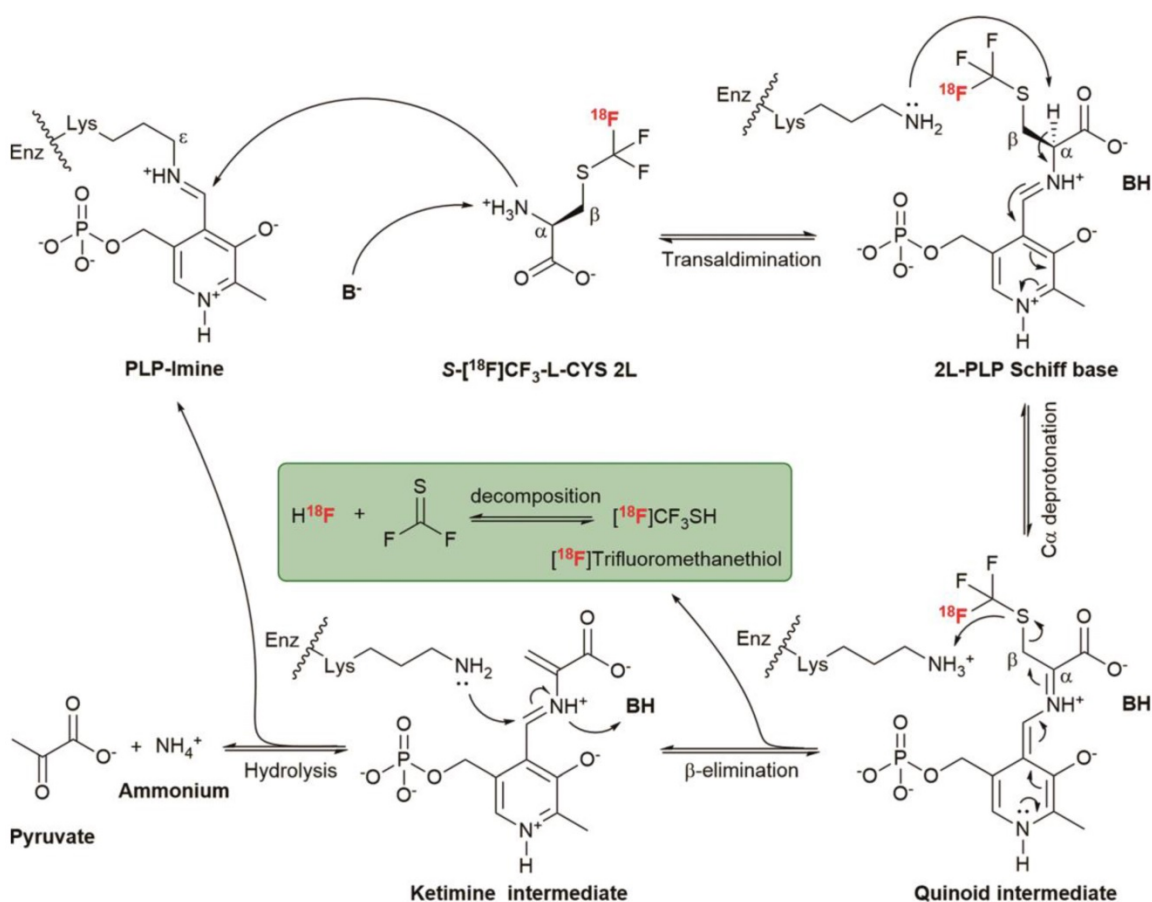


**Figure 4.** (A) The biodistribution of 2L in normal Kunming mice at 5, 30, 60 and 90 min post-injection; (B) The biodistribution of 2D in normal Kunming mice at 5, 30, 60 and 90 min post-injection.



**Scheme 2.** Possible mechanism of cysteine  $S$ -conjugate  $\beta$ -lyases catalyzed  $\beta$ -elimination of  $S$ -[ $^{18}\text{F}$ ]CF $_3$ -L-CYS **2L**. PLP, the biologically active cofactor, is bound to the enzyme (Enz) at the  $\epsilon$ -amino group of the lysine residue.

### **In vivo PET imaging of $S$ -[ $^{18}\text{F}$ ]CF $_3$ -D-CYS**

The promising results from *in vitro* cell uptake studies and *in vivo* biodistribution studies, such as specific tumor-targeting properties and favourable pharmacokinetic characteristics, inspired us to further investigate the feasibility of **2D** as an amino acid tracer for glioma PET imaging. As shown in **Figure 5A**, the D-enantiomer selectively accumulated in C6 tumor tissues to give a good tumor-to-background contrast, which was predominantly cleared by renal excretion with moderate liver accumulation. The average uptake values of **2D** in the tumor were  $3.81 \pm 0.23$ ,  $3.74 \pm 0.18$ ,  $3.56 \pm 0.15\%$  ID/g ( $n = 3$ ) at 45, 60 and 75 min after injection, respectively. Compared with [ $^{18}\text{F}$ ]FDG, **2D** exhibited relative less tumor radioactivity accumulation but much lower uptake in most major organs (except of pancreas, kidney and bladder), particularly in normal brain tissue (**Figure 5A-B**). Hence, the tumor-to-brain uptake ratio of **2D** was substantially higher than that of [ $^{18}\text{F}$ ]FDG (**Figure 5C**). In addition, a slightly high **2D** uptake was observed in the muscle tissues, which might restrict the application of the D-enantiomer in regions beyond the brain.

To further determine the distribution patterns of **2D**, a 90 min dynamic micro-PET scan was performed in other C6-bearing mice (**Figure S6**). The time-activity curves were obtained from dynamic images after drawing regions of interest (**Figure 6A**). Relative uptake ratios of tumor-to-brain, tumor-to-muscle and tumor-to-bone at different time points were then calculated and illustrated in **Figure 6B**. During the first 30 min, **2D** reached its maximum uptake value and exhibited a long-term retention in the C6 tumor, then declined slowly. The highest tumor-to-brain uptake ratio of 14.70 was achieved at 15 min after injection of **2D**. It was also noteworthy that the bone uptake increased slightly as time went on, which was consistent with the results of the biodistribution studies. Even so, several competing factors should be considered synthetically in the process of defining PET images, such as tumor tissue uptake, *in vivo* defluorination or bone marrow accumulation, and pharmacokinetic characteristics [74]. Additional investigations are warranted in the future to ascertain *in vivo* metabolic fate of the  $^{18}\text{F}$ -trifluoromethylated cysteines as well as their stability *in vitro* in the presence of the cysteine  $S$ -conjugate  $\beta$ -lyases. Taken together, these results

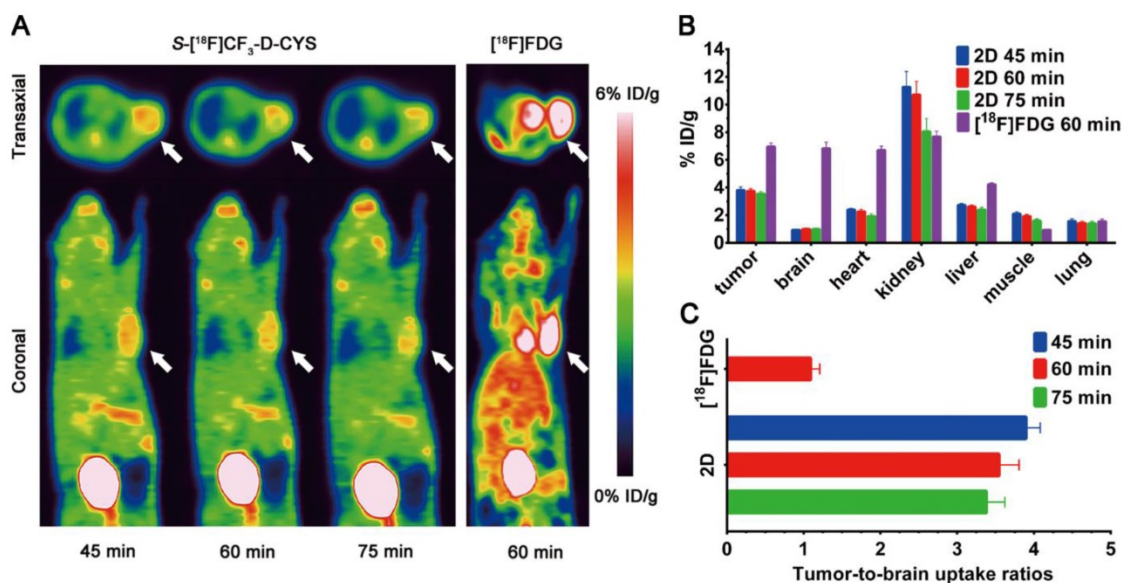


**Figure 5.** (A) Static micro-PET images of C6 glioma-bearing mice scanned at 45, 60 and 75 min after injection of S-[<sup>18</sup>F]CF<sub>3</sub>-D-CYS **2D** and at 60 min after injection of [<sup>18</sup>F]FDG (the white arrow indicates the tumor); (B) Image-derived biodistribution data of **2D** (at 45, 60 and 75 min post-injection) and [<sup>18</sup>F]FDG (at 60 min post-injection) in most major organs and tumor; (C) Comparison of tumor-to-brain uptake ratios between **2D** and [<sup>18</sup>F]FDG at different time points post-injection.

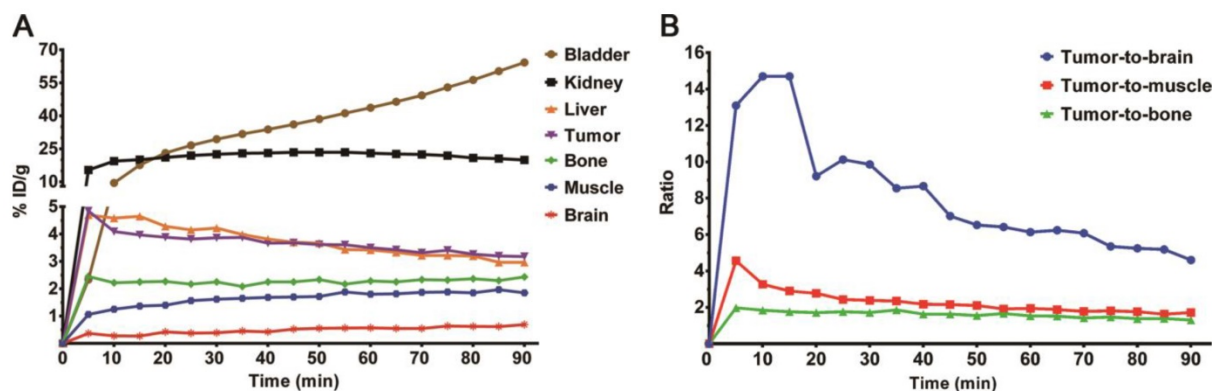


**Figure 6.** (A) Time-activity curves of brain, muscle, bone, tumor, liver, kidney and bladder uptake in BALB/c nude mice bearing C6 tumor after injection of **2D**; (B) Relative uptake ratios of tumor-to-brain, tumor-to-muscle and tumor-to-bone at different time points (0 to 90 min) after injection of **2D**.

showed that S-[<sup>18</sup>F]CF<sub>3</sub>-D-CYS **2D**, an [<sup>18</sup>F]CF<sub>3</sub>-functionalized SAA tracer, might be a potential candidate for glioma imaging.

## Conclusions

In conclusion, we have successfully designed and synthesized a couple of <sup>18</sup>F-trifluoromethylated cysteine enantiomers (**2L** and **2D**) according to a structure-based bioisosterism strategy. *In vitro* study indicated that cellular uptake of the two enantiomers was primarily associated with AA transport systems L and ASC. Notably, *in vivo* biodistribution and PET imaging studies demonstrated that **2D** was characterized with relatively good stability and high tumor-specific accumulation. Our results suggest that <sup>18</sup>F-trifluoromethylated D-cysteine, a new SAA tracer, may be a potential candidate for PET imaging of glioma. To the best of our knowledge, this is the first study to synthesize enantiopure <sup>18</sup>F-trifluoromethylated cysteines and to evaluate their feasibility as

“structure-mimetic” AA tracers for tumor imaging. Also, a more detailed biological evaluation is underway.

## Materials and Methods

### Radiochemistry

<sup>18</sup>F-fluoride was trapped on a QMA light cartridge and subsequently eluted by a H<sub>2</sub>O/CH<sub>3</sub>CN (1:9, 1.0 mL) mixed solution of K<sub>2</sub>CO<sub>3</sub> (3 mg) and K<sub>2.2.2</sub> (13 mg) into a sealed penicillin bottle (10 mL). The K<sub>2.2.2</sub>/K<sup>18</sup>F solution was evaporated at 95 °C for 10 min under a N<sub>2</sub> flow and resolubilized in anhydrous CH<sub>3</sub>CN (1.0 mL). The resulting solution of K<sub>2.2.2</sub>/K<sup>18</sup>F in anhydrous CH<sub>3</sub>CN was entirely transferred into a 10 mL volumetric penicillin bottle (sealed by a rubber cap) containing the cyclic-sulfamidate precursor (**3L** or **3D**; 2 mg, 6 μmol), PDFA (1.5 mg, 6 μmol) and S<sub>8</sub> (3.0 mg, 12 μmol). The nucleophilic <sup>18</sup>F-trifluoromethylthiolation reaction was carried out

at 70 °C for 5 min without electromagnetic stirring. After the reaction completed, the reaction mixture was diluted by 5% AcOH aqueous solution (10 mL) and passed through a C18 plus short cartridge. After washed by sterilized water (10 mL), the <sup>18</sup>F-labelled intermediate **4L** or **4D** was eluted from C18 cartridge by ethanol (1.5 mL) into another sealed penicillin bottle. The solvent was removed by evaporation at 85 °C for 5 min under a N<sub>2</sub> flow. 4 N HCl aq. (0.8 mL) was added to the residue and heated for 10 min at 90 °C. Finally, the product (**2L** or **2D**) was purified by passing serially through an AG 11 A8 ion retardation resin column, a Sep-Pak alumina N plus light cartridge, a C18 plus short cartridge, and a sterile Millipore 0.22 μm filter with 0.9% NaCl aq. solution (2 mL) into a final product vial (pH ≈ 6).

A detailed descriptions of all experimental procedures, including organic chemistry synthesis, radiochemistry synthesis, and *in vitro* and *in vivo* biological evaluation experiments, can be found in the Supplementary Materials.

## Abbreviations

AAs: Amino acids; PET: Positron emission tomography; SAAs: Sulfur-containing amino acids; DNA: Deoxyribonucleic acid; [<sup>11</sup>C]MET: L-methyl-<sup>11</sup>C-methionine; [<sup>18</sup>F]FDG: 2-[<sup>18</sup>F]fluoro-2-deoxy-D-glucose; S-[<sup>11</sup>C]CH<sub>3</sub>-L-CYS: S-[<sup>11</sup>C]-methyl-L-cysteine; S-[<sup>11</sup>C]CH<sub>3</sub>-D-CYS: S-[<sup>11</sup>C]-methyl-D-cysteine; MEP: Molecular electrostatic potential; S-CF<sub>3</sub>-L-CYS: S-trifluoromethyl-L-cysteine; S-CF<sub>3</sub>-D-CYS: S-trifluoromethyl-D-cysteine; -CO<sub>2</sub><sup>-</sup>: Carboxylate group; -BF<sub>3</sub><sup>-</sup>: Trifluoroborate group; -CF<sub>3</sub>: Trifluoromethyl group; -CH<sub>3</sub>: Methyl group; -SCF<sub>3</sub>: Trifluoromethylthio group; PDFA: Difluoromethylene phosphobetaine (Ph<sub>3</sub>P<sup>+</sup>CF<sub>2</sub>CO<sub>2</sub><sup>-</sup>); S<sub>8</sub>: Elemental sulfur; aq.: Aqueous; RCY: Radiochemical yield; TLC: Thin-layer chromatography; HPLC: High performance liquid chromatography; BCH: 2-amino-2-norbornanecarboxylic acid; Ser: L-serine; MeAIB: 2-aminoisobutyric acid; L-MCYS: S-methyl-L-cysteine; TCA: Trichloroacetic acid; B: Deprotonated base; PLP: Pyridoxal 5'-phosphate; [<sup>18</sup>F]CF<sub>3</sub>SH: [<sup>18</sup>F]Trifluoromethanethiol; Enz: Enzyme.

## Supplementary Material

Supplementary information, figures and tables.  
<http://www.thno.org/v09p1144s1.pdf>

## Acknowledgements

This work was supported in part by the National Natural Science Foundation of China (NSFC) (Nos. 81571704 to G. Tang), the Science and Technology Foundation of Guangdong Province (Nos. 2016B090920087, 2014A020210008 to G. Tang), the

Science and Technology Planning Project Foundation of Guangzhou (No. 201604020169 to G. Tang), the National Natural Science Foundation of China (NSFC) (No. 81703343 to G. Yang), a General Financial Grant from the Natural Science Foundation of Tianjin-China (No. 16JCQNJC13300 to G. Yang), Fundamental Research Funds for the Central Universities to G. Yang, China Postdoctoral Science Foundation (CPSF) (No. 2018M631029 to S. Liu).

## Author Contributions

S. Liu designed the study, synthesized the compounds and wrote the original manuscript. S. Liu, H. Ma, Z. Zhang, L. Lin, and G. Yuan conducted the cell and animal experiments. X. Tang, D. Nie, and S. Jiang discussed the results and analysed the data. G. Yang supervised the studies in synthetic chemistry, discussed the results and revised the paper. G. Tang supervised the project, discussed the results, analysed the data and revised the paper. All authors read and approved the manuscript.

## Competing Interests

The authors have declared that no competing interest exists.

## References

- Christensen HN. Role of amino acid transport and countertransport in nutrition and metabolism. *Physiol Rev.* 1990; 70: 43-77.
- Fotiadis D, Kanai Y, Palacin M. The SLC3 and SLC7 families of amino acid transporters. *Mol Aspects Med.* 2013; 34: 139-58.
- Yanagida O, Kanai Y, Chairoungdua A, Kim DK, Segawa H, Nii T, et al. Human L-type amino acid transporter 1 (LAT1): Characterization of function and expression in tumor cell lines. *Biochim Biophys Acta.* 2001; 1514: 291-02.
- Fuchs BC, Bode BP. Amino acid transporters ASCT2 and LAT1 in cancer: Partners in crime? *Semin Cancer Biol.* 2005; 15: 254-66.
- Kobayashi K, Ohnishi A, Promsuk J, Shimizu S, Kanai Y, Shiohara Y, et al. Enhanced tumor growth elicited by L-type amino acid transporter 1 in human malignant glioma cells. *Neurosurgery.* 2008; 62: 493-03.
- Ganapathy V, Thangaraju M, Prasad PD. Nutrient transporters in cancer: Relevance to Warburg hypothesis and beyond. *Pharmacol Ther.* 2009; 121: 29-40.
- Shimizu K, Kaira K, Tomizawa Y, Sunaga N, Kawashima O, Oriuchi N, et al. ASC amino-acid transporter 2 (ASCT2) as a novel prognostic marker in non-small cell lung cancer. *Br J Cancer.* 2014; 110: 2030-9.
- Bhutia YD, Babu E, Ramachandran S, Ganapathy V. Amino Acid transporters in cancer and their relevance to "glutamine addiction": Novel targets for the design of a new class of anticancer drugs. *Cancer Res.* 2015; 75: 1782-8.
- Cormerais Y, Massard PA, Vucetic M, Giuliano S, Tambutte E, Durivault J, et al. The glutamine transporter ASCT2 (SLC1A5) promotes tumor growth independently of the amino acid transporter LAT1 (SLC7A5). *J Biol Chem.* 2018; 293: 2877-87.
- Laverman P, Boerman OC, Corstens FH, Oyen WJ. Fluorinated amino acids for tumour imaging with positron emission tomography. *Eur J Nucl Med Mol Imaging.* 2002; 29: 681-90.
- McConathy J, Goodman MM. Non-natural amino acids for tumor imaging using positron emission tomography and single photon emission computed tomography. *Cancer Metast Rev.* 2008; 27: 555-73.
- McConathy J, Yu WP, Jarkas N, Seo W, Schuster DM, Goodman MM. Radiohalogenated nonnatural amino acids as PET and SPECT tumor imaging agents. *Med Res Rev.* 2012; 32: 868-905.
- Kong FL, Yang DJ. Amino acid transporter-targeted radiotracers for molecular imaging in oncology. *Curr Med Chem.* 2012; 19: 3271-81.
- Huang C, McConathy J. Radiolabeled amino acids for oncologic imaging. *J Nucl Med.* 2013; 54: 1007-10.
- Langen KJ, Watts C. Neuro-oncology: Amino acid PET for brain tumours - ready for the clinic? *Nat Rev Neurol.* 2016; 12: 375-6.
- Langen KJ, Galldiks N, Hattingen E, Shah NJ. Advances in neuro-oncology imaging. *Nat Rev Neurol.* 2017; 13: 279-89.

17. Sun A, Liu X, Tang G. Carbon-11 and fluorine-18 labeled amino acid tracers for positron emission tomography imaging of tumors. *Front Chem.* 2017; 5: 124.
18. Ametamey SM, Honer M, Schubiger PA. Molecular imaging with PET. *Chem Rev.* 2008; 108: 1501-16.
19. Scott PJ. Methods for the incorporation of carbon-11 to generate radiopharmaceuticals for PET imaging. *Angew Chem.* 2009; 48: 6001-4.
20. Rotstein BH, Liang SH, Placzek MS, Hooker JM, Gee AD, Dolle F, et al.  $^{11}\text{C}=\text{O}$  bonds made easily for positron emission tomography radiopharmaceuticals. *Chem Soc Rev.* 2016; 45: 4708-26.
21. Pekosak A, Filip U, Poot AJ, Windhorst AD. From carbon-11-labeled amino acids to peptides in positron emission tomography: the synthesis and clinical application. *Mol Imaging Biol.* 2018; 20: 510-32.
22. Brosnan JT, Brosnan ME. The sulfur-containing amino acids: An overview. *J Nutr.* 2006; 136 (Suppl 6): S1636-40.
23. Herholz K, Hölzer T, Bauer B, Schröder R, Voges J, Ernestus RI, et al.  $^{11}\text{C}$ -methionine PET for differential diagnosis of low-grade gliomas. *Neurology.* 1998; 50: 1316-22.
24. Chung JK, Yu K, Kim S, Yong L, Paek S, Yeo J, et al. Usefulness of  $^{11}\text{C}$ -methionine PET in the evaluation of brain lesions that are hypo- or isometabolic on  $^{18}\text{F}$ -FDG PET. *Eur J Nucl Med Mol Imaging.* 2002; 29: 176-82.
25. Weber WA, Wester HJ, Grosu AL, Herz M, Dzewas B, Feldmann HJ, et al.  $O$ -(2- $^{18}\text{F}$ fluoroethyl)-L-tyrosine and L-methyl- $^{11}\text{C}$ methionine uptake in brain tumours: initial results of a comparative study. *Eur J Nucl Med.* 2000; 27: 542-9.
26. Glaudemans AW, Enting RH, Heesters MA, Dierckx RA, van Rheenen RW, Walenkamp AM, et al. Value of  $^{11}\text{C}$ -methionine PET in imaging brain tumours and metastases. *Eur J Nucl Med Mol Imaging.* 2013; 40: 615-35.
27. Herholz K. Brain Tumors: An update on clinical PET research in gliomas. *Semin Nucl Med.* 2017; 47: 5-17.
28. Terakawa Y, Tsuyuguchi N, Iwai Y, Yamanaka K, Higashiyama S, Takami T, et al. Diagnostic accuracy of  $^{11}\text{C}$ -methionine PET for differentiation of recurrent brain tumors from radiation necrosis after radiotherapy. *J Nucl Med.* 2008; 49: 694-9.
29. Ullrich RT, Kracht L, Brunn A, Herholz K, Frommolt P, Miletic H, et al. L-methyl- $^{11}\text{C}$ methionine PET as a diagnostic marker for malignant progression in patients with glioma. *J Nucl Med.* 2009; 50: 1962-8.
30. Yasukawa T, Yoshikawa K, Aoyagi H, Yamamoto N, Tamura K, Suzuki K, et al. Usefulness of PET with  $^{11}\text{C}$ -methionine for the detection of hilar and mediastinal lymph node metastasis in lung cancer. *J Nucl Med.* 2000; 41: 283-90.
31. Kubota K. From tumor biology to clinical PET: A review of positron emission tomography (PET) in oncology. *An Nucl Med.* 2001; 15: 471-86.
32. Sasaki M, Kuwabara Y, Yoshida T, Nakagawa M, Koga H, Hayashi K, et al. Comparison of MET-PET and FDG-PET for differentiation between benign lesions and malignant tumors of the lung. *An Nucl Med.* 2001; 15: 425-31.
33. Maeda Y, Oguni H, Saitou Y, Mutoh A, Imai K, Osawa M, et al. Rasmussen syndrome: multifocal spread of inflammation suggested from MRI and PET findings. *Epilepsia.* 2003; 44: 1118-21.
34. Ishiwata K. Metabolic fate of L-methyl- $^{11}\text{C}$ methionine in human plasma. *Eur J Nucl Med.* 1989; 15: 665-9.
35. Deng HF, Tang XL, Wang HL, Tang GH, Wen FH, Shi XC, et al. S- $^{11}\text{C}$ -methyl-L-cysteine: A new amino acid PET tracer for cancer imaging. *J Nucl Med.* 2011; 52: 287-93.
36. Huang TT, Tang GH, Wang HL, Nie DH, Tang XL, Liang X, et al. Synthesis and preliminary biological evaluation of S- $^{11}\text{C}$ -methyl-D-cysteine as a new amino acid PET tracer for cancer imaging. *Amino Acids.* 2015; 47: 719-27.
37. Tang GH, Tang XL, Deng HF, Wang HL, Wen FH, Yi C, et al. Efficient preparation of  $^{11}\text{C}$ CH<sub>3</sub>Br for the labeling of  $^{11}\text{C}$ CH<sub>3</sub>-containing tracers in positron emission tomography clinical practice. *Nucl Med Commun.* 2011; 32: 466-74.
38. Yao BG, Tang CH, Tang GH, Hu KZ, Liang X, Shi XC, et al. Human Biodistribution and radiation dosimetry of S- $^{11}\text{C}$ -methyl-L-cysteine using whole-body PET. *Clin Nucl Med.* 2015; 40: e470-4.
39. Parente A, Waarde AV, Shoji A, Faria DDP, Maas B, Zijlma R, et al. PET imaging with S- $^{11}\text{C}$ -methyl-L-cysteine and L-methyl- $^{11}\text{C}$ methionine in rat models of glioma, glioma radiotherapy, and neuroinflammation. *Mol Imaging Biol.* 2017; 20: 1-8.
40. Huang TT, Wang HL, Tang GH, Liang X, Nie DH, Yi C, et al. A comparative uptake study of multiplexed PET tracers in mice with turpentine-induced inflammation. *Molecules.* 2012; 17: 13948-59.
41. Tang GH, Wang MF, Tang XL, Luo L, Gan MQ. Fully automated synthesis module for preparation of S-(2- $^{18}\text{F}$ fluoroethyl)-L-methionine by direct nucleophilic exchange on a quaternary 4-aminopyridinium resin. *Nucl Med Biol.* 2003; 30: 509-12.
42. Bourdier T, Fookes CJR, Pham TQ, Greguric I, Katsifis A. Synthesis and stability of S-(2- $^{18}\text{F}$ fluoroethyl)-L-homocysteine for potential tumour imaging. *J Labelled Compd Radiopharm.* 2008; 51: 369-73.
43. Bourdier T, Shepherd R, Berghofer P, Jackson T, Fookes CJ, Denoyer D, et al. Radiosynthesis and biological evaluation of L- and D-S-(3- $^{18}\text{F}$ fluoropropyl)homocysteine for tumor imaging using positron emission tomography. *J Med Chem.* 2011; 54: 1860-70.
44. Denoyer D, Kirby L, Waldeck K, Roselt P, Neels OC, Bourdier T, et al. Preclinical characterization of  $^{18}\text{F}$ -D-FPHCys, a new amino acid-based PET tracer. *Eur J Nucl Med Mol Imaging.* 2012; 39: 703-12.
45. Yang XY, Liu ZB, Zhang HM, Li Z, Munasinghe JP, Niu G, et al. Preclinical evaluation of an  $^{18}\text{F}$ -trifluoroborate methionine derivative for glioma imaging. *Eur J Nucl Med Mol Imaging.* 2018; 45: 585-92.
46. Muller K, Faeh C, Diederich F. Fluorine in pharmaceuticals: looking beyond intuition. *Science.* 2007; 317: 1881-6.
47. Purser S, Moore PR, Swallow S, Gouverneur V. Fluorine in medicinal chemistry. *Chem Soc Rev.* 2008; 37: 320-30.
48. Hagmann WK. The many roles for fluorine in medicinal chemistry. *J Med Chem.* 2008; 51: 4359-69.
49. Meanwell NA. Synopsis of some recent tactical application of bioisosteres in drug design. *J Med Chem.* 2011; 54: 2529-91.
50. Chu LL, Qing FL. Oxidative trifluoromethylation and trifluoromethylthiolation reactions using (trifluoromethyl)trimethylsilane as a nucleophilic CF<sub>3</sub> source. *Acc Chem Res.* 2014; 47: 1513-22.
51. Kieltch I, Eisenberger P, Togni A. Mild electrophilic trifluoromethylation of carbon- and sulfur-centered nucleophiles by a hypervalent iodine(III)-CF<sub>3</sub> reagent. *Angew Chem.* 2007; 46: 754-7.
52. Capone S, Kieltch I, Flögel O, Lelais G, Togni A, Seebach D. Electrophilic S-trifluoromethylation of cysteine side chains in  $\alpha$ - and  $\beta$ -peptides: Isolation of trifluoro-methylated Sandostatin® (octreotide) derivatives. *Helv Chim Acta.* 2008; 91: 2035-56.
53. Umemoto T, Ishihara S. Power-variable electrophilic trifluoromethylating agents. S-, Se-, and Te-(trifluoromethyl)dibenzothio-, -seleno-, and -tellurophenium salt system. *J Am Chem Soc.* 1993; 115: 2156-64.
54. Verhoog S, Kee CW, Wang Y, Khotavivattana T, Wilson TC, Kersemans V, et al.  $^{18}\text{F}$ -trifluoromethylation of unmodified peptides with 5- $^{18}\text{F}$ -(trifluoromethyl)dibenzothiophenium trifluoromethanesulfonate. *J Am Chem Soc.* 2018; 140: 1572-5.
55. Zheng J, Wang L, Lin JH, Xiao JC, Liang SH. Difluorocarbene-derived trifluoromethylthiolation and  $^{18}\text{F}$ trifluoromethylthiolation of aliphatic electrophiles. *Angew Chem.* 2015; 54: 13236-40.
56. Zheng J, Cheng R, Lin JH, Yu DH, Ma L, Jia L, et al. An unconventional mechanistic insight into SCF<sub>3</sub> formation from difluorocarbene: Preparation of  $^{18}\text{F}$ -labeled  $\alpha$ -SCF<sub>3</sub> carbonyl compounds. *Angew Chem.* 2017; 56: 3196-200.
57. Zeng JL, Chachignon H, Ma JA, Cahard D. Nucleophilic trifluoromethylthiolation of cyclic sulfamidates: Access to chiral  $\beta$ - and  $\gamma$ -SCF<sub>3</sub> amines and  $\alpha$ -amino esters. *Org Lett.* 2017; 19: 1974-7.
58. Baldwin JE, Spivey AC, Schofield CJ. Cyclic sulphamidates: New synthetic precursors for  $\beta$ -functionalised  $\alpha$ -amino acids. *Tetrahedron: Asymmetry.* 1990; 1: 881-4.
59. Halcomb SBCARL. Application of serine- and threonine-derived cyclic sulfamidates for the preparation of S-linked glycosyl amino acids in solution- and solid-phase peptide synthesis. *J Am Chem Soc.* 2002; 124: 2534-43.
60. Yu WP, McConathy J, Williams L, Camp VM, Malveaux EJ, Zhang ZB, et al. Synthesis, radiolabeling, and biological evaluation of (R)- and (S)-2-amino-3- $^{18}\text{F}$ fluoro-2-methylpropanoic acid (FAMP) and (R)- and (S)-3- $^{18}\text{F}$ fluoro-2-methyl-2-N-(methylamino)propanoic acid (NMeFAMP) as potential PET radioligands for imaging brain tumors. *J Med Chem.* 2010; 53: 876-86.
61. McConathy J, Martarello L, Malveaux EJ, Camp VM, Simpson NE, Simpson CP, et al. Radiolabeled amino acids for tumor imaging with PET: Radiosynthesis and biological evaluation of 2-amino-3- $^{18}\text{F}$ fluoro-2-methylpropanoic acid and 3- $^{18}\text{F}$ fluoro-2-methyl-2-(methylamino)propanoic acid. *J Med Chem.* 2002; 45: 2240-9.
62. Yu WP, Williams L, Camp VM, Olson JJ, Goodman MM. Synthesis and biological evaluation of anti-1-amino-2- $^{18}\text{F}$ fluoro-cyclobutyl-1-carboxylic acid (anti-2- $^{18}\text{F}$  FACBC) in rat 9L gliosarcoma. *Bioorg Med Chem Lett.* 2010; 20: 2140-3.
63. Pippin AB, Voll RJ, Li YC, Wu H, Mao H, Goodman MM. Radiochemical synthesis and evaluation of  $^{15}\text{N}$ -labeled 5-aminolevulinic acid for PET imaging of gliomas. *ACS Med Chem Lett.* 2017; 8: 1236-40.
64. Gadais C, Saraiva-Rosa N, Chelain E, Pytkowicz J, Brigaud T. Tailored approaches towards the synthesis of L-S-(trifluoromethyl)cysteine- and L-trifluoromethionine-containing peptides. *Eur J Org Chem.* 2017; 2017: 246-51.
65. Wu ZH, Zha ZH, Li GX, Lieberman BP, Choi SR, Ploessl K, et al. (2S,4S)-4-(3- $^{18}\text{F}$ fluoropropyl)glutamine as a tumor imaging agent. *Molecular pharmacology.* 2014; 11: 3852-66.
66. Urakami T, Sakai K, Asai T, Dai F, Tsukada H, Oku N. Evaluation of O- $^{18}\text{F}$ fluoromethyl-D-tyrosine as a radiotracer for tumor imaging with positron emission tomography. *Nucl Med Biol.* 2009; 36: 295-03.
67. Cooper AJ, Pinto JT. Cysteine S-conjugate  $\beta$ -lyases. *Amino Acids.* 2006; 30: 1-15.
68. Cooper AJ, Krasnikov BF, Pinto JT, Bruschi SA. Measurement of cysteine S-conjugate  $\beta$ -lyase activity. In: Maines MD, Ed. *Curr Protoc Toxicol.* 2010; 44:4.36.1-4.36.18.
69. Cooper AJ, Younis IR, Niatsetskaia ZV, Krasnikov BF, Pinto JT, Petros WP, et al. Metabolism of the cysteine S-conjugate of busulfan involves a  $\beta$ -Lyase reaction. *Drug Metab Dispos.* 2008; 36: 1546-52.
70. Clausen T, Huber R, Messerschmidt A, Pohlentz H-D, Laber B. Slow-binding inhibition of escherichia coli cystathionine  $\beta$ -lyase by L-aminoethoxyvinylglycine: A kinetic and X-ray study. *Biochem.* 1997; 36: 12633-43.

71. Metzler CM , Harris AG , Metzler DE. Spectroscopic studies of quinonoid species from pyridoxal 5'-phosphate. *Biochem.* 1988; 27: 4923.
72. Clausen T, Huber R, Laber B, Pohlenz HD, Messerschmidt A. Crystal structure of the pyridoxal-5'-phosphate dependent cystathionine  $\beta$ -lyase from *escherichia coli* at 1.83 Å. *J Mol Biol.* 1996; 262: 202-24.
73. Cooper AJL, Krasnikov BF, Niatsetskaya ZV, Pinto JT, Callery PS, Villar MT, et al. Cysteine S-conjugate  $\beta$ -lyases: Important roles in the metabolism of naturally occurring sulfur and selenium-containing compounds, xenobiotics and anticancer agents. *Amino Acids.* 2011; 41: 7-27.
74. Ploessl K, Wang LM, Lieberman BP, Qu WC, Kung HF. Comparative evaluation of  $^{18}\text{F}$ -labeled glutamic acid and glutamine as tumor metabolic imaging agents. *J Nucl Med.* 2012; 53: 1616-24.